Propagation Analysis of Signal Fading for Basic Exchange Radios

Jean-Fu Kiang, *Member, IEEE*, and Sing H. Lin, *Senior Member, IEEE*

Abstract—**Advances in microelectronics, digital radio, and voice coding technologies make basic exchange radio (BEXR) systems economically attractive for rural telecommunications services. The performance and reliability of a BEXR can be affected by multipath fading. Although empirical multipath fading models are available for microwave links above 2 GHz, these models are not directly applicable to the BEXR links because of the substantial differences in frequency, antenna beamwidth, and radio path clearance. In this paper, we present a method to obtain a scaling factor which accounts for the differences between BEXR and microwave links. First, we study the terrain scattering by using a rough surface model and the atmospheric refraction by using a ray tracing approach. Then, we calculate the received signal powers of a microwave link and two BEXR links on the same path under the same propagation condition. The signal characteristics are investigated and used to simulate the fading distributions for all three links. From the simulation results, we derive a scaling factor to modify the existing microwave multipath fading models for BEXR application. The predictions by the modified model agree well with measured BEXR data. This study shows that probability distribution of signal fading on BEXR links is a strong function of antenna height and beamwidth.**

I. Introduction

BOTH the initial capital and the ongoing maintenance costs can be significant if cables or open wires are used to provide telecommunications services to dispersed subscribers in rural areas. Advances in microelectronics, digital radio, and voice coding technologies make basic exchange radio (BEXR) systems economically attractive for providing rural telecommunications services. Frequencies for BEXR in the United States are in the 150 MHz, 450 MHz, and 800 MHz bands [1]–[3]. The deployment of BEXR systems is accelerating worldwide, providing affordable telephone service to rural residents.

The performance and reliability of a BEXR link are affected by anomalous atmospheric radio propagation conditions such as multipath fading and obstruction fading [4]–[6]. Since severe fading can degrade service quality or cause outages to BEXR links, models of fading signals are needed to engineer these links and meet performance and reliability objectives.

Empirical signal fading models for microwave links above 2 GHz may not be directly applicable to BEXR links because of the substantial differences in operating frequency, antenna beamwidth, and path clearance. The antenna beamwidth of a typical microwave link is 3° or less whereas the antenna of a BEXR radio base station is usually omnidirectional in the horizontal plane. Furthermore, microwave radio links usually use high radio towers (for example, 75 m) to obtain a clear path whereas the BEXR links have little path clearance because the antenna poles at the subscriber sites are usually short (15 m or less). These differences cause significantly different signal fading characteristics [7], [8].

In [9], experiments were carried out to study the radio propagation properties affected by the refractivity. In [10]–[12], ray tracing approaches were used to study the multipath propagation caused by atmospheric refraction. In [11] and [12], terrain reflection is accounted for by a reflection coefficient at the specular point. These studies were carried out for microwave links in which the terrain scattering is not significant owing to the narrow antenna beamwidth.

Recently, we completed a preliminary statistical analysis on measured fading data for two BEXR links [13]. The results show that signal fading on those two links may be largely caused by multipath fading. Because of the wide beamwidth of antennas used in the BEXR, we need to investigate both the terrain scattering and the atmospheric refraction to fully understand the fading characteristics of BEXR. In Section II, we present a rough surface model to study the terrain scattering. In Section III, we describe a ray tracing approach to study the atmospheric refraction. In Section IV, empirical microwave models of fading distribution are reviewed. In Section V, we present the results on BEXR links by the rough surface model and the ray tracing approach. In Section VI, we use the received signal characteristics to simulate the fading distributions for a microwave link and two BEXR links. By comparing these fading distributions, we obtain a scaling factor to modify the existing microwave multipath fading models for BEXR applications.

II. Rough Surface Model

In this section, we give a brief review of the two-dimensional rough surface model by Beckmann and Spizzichino [14]. As shown in Fig. 1, $\overline{E}_i$ is the incident field and $\overline{E}_s(\overline{r})$ is the field at $\overline{r}$ caused by scattering from surface area A. $\overline{E}_r(\overline{r}_0)$ is the reference field at $\overline{r}_0$ due to specular reflection from the same surface area A as if the surface were smooth. Here, $\overline{r}'_0$ is the center coordinate of the area A, and $|\overline{r} - \overline{r}'_0| = |\overline{r}_0 - \overline{r}'_0|$. We define the ratio of $|\overline{E}_s(\overline{r})|$ and $|\overline{E}_r(\overline{r}_0)|$ as

$$\rho(\overline{r}, A) = |\overline{E}_s(\overline{r})| / |\overline{E}_r(\overline{r}_0)|. \quad (1)$$

Manuscript received December 26, 1991; revised March 8, 1993.

J.-F. Kiang was with Bell Communications Research, Red Bank, NJ 07701. He is now with Siemens Medical Electronics, Inc., 16 Electronics Ave., Danvers, MA 01923.

S. H. Lin is with Bell Communications Research, 100 Schultz Drive, Red Bank, NJ 07701.

IEEE Log Number 9211250.

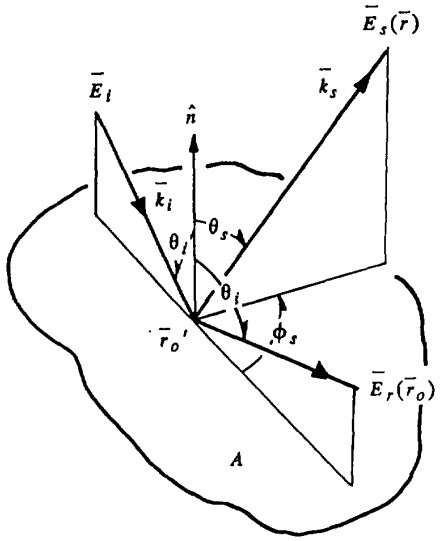

Fig. 1. Geometry of terrain scattering by surface area A. $\bar{E}_i$ is the incident field, $\bar{E}_s$ is the scattered field, and $\bar{E}_r$ is the specularly reflected field.

We assume that the reflection coefficient within A can be approximated by an averaged coefficient; then $\rho(\bar{r}, A)$ can be approximated as

$$\rho(\bar{r}, A) \approx F(\theta_i, \theta_s, \phi_s)(1/a) \int_A \int d\bar{r}' e^{i\bar{v}\cdot(\bar{r}'-\bar{r}_0')}, \quad (2)$$

where a is the area of A, $\bar{v} = \bar{k}_i - \bar{k}_s$, $\bar{k}_i$ ($\bar{k}_s$) is the wave number vector of the incident (scattering) wave, and $F(\theta_i, \theta_s, \phi_s)$ is a factor which depends on the incident and the scattering angles.

Next, we choose A to be a rectangle of $2l_x$ by $2l_y$ with $l_x \gg \lambda$ and $l_y \gg \lambda$. The local coordinate of the terrain surface within A is defined as $\bar{r}' - \bar{r}_0' = x\hat{x} + y\hat{y} + \zeta\hat{z}$. Then, the ensemble average of $\rho(\bar{r}, A)$ can be represented as

$$\langle\rho\rangle \approx F(\theta_i, \theta_s, \phi_s)\chi(v_z)\rho_0(l_x, l_y). \quad (3)$$

Here, $\chi(v_z)$ is the characteristic function of the distribution $w(\zeta)$ for terrain roughness ζ, and

$$\rho_0(l_x, l_y) = \operatorname{sinc}(v_x l_x)\operatorname{sinc}(v_y l_y), \quad (4)$$

where $\operatorname{sinc}(\alpha) = \sin\alpha/\alpha$.

The variance of ρ can be expressed as

$$D(\rho) = (\pi/a)T^2F^2e^{-g}\sum_{m=1}^{\infty}\frac{g^m}{m!m}\exp\left(-v_\tau^2T^2/4m\right), \quad (5)$$

where $v_\tau = \sqrt{v_x^2 + v_y^2}$, T is the correlation distance of the terrain, and

$$g = (v_z\sigma)^2 = [k_0\sigma(\cos\theta_i + \cos\theta_s)]^2, \quad (6)$$

where σ is the standard deviation of the terrain roughness.

For microwave and BEXR links with frequencies below 1 GHz, we have $g \ll 1$ within the illuminated area. Thus, (5) can be approximated by the first term, and

$$\begin{aligned}\langle\rho\rho^*\rangle &= D(\rho) + \langle\rho\rangle\langle\rho^*\rangle \\ &\approx e^{-g}F^2\left[\rho_0^2 + \frac{\pi gT^2}{a}\exp\left(-v_\tau^2T^2/4\right)\right]. \end{aligned} \quad (7)$$

From (1) and (7), the scattered power contributed by A can be expressed as

$$\begin{aligned}P_s(A) &= \frac{1}{\eta_0}\langle E_s(\bar{r})E_s^*(\bar{r})\rangle_A \\ &= \frac{P_t(a/\lambda)^2}{2\pi r_i^2 r_s^2}G_t(\theta_t, \phi_t)G_r(\theta_r, \phi_r) \\ &\quad\cdot\cos^2\theta_i F^2 e^{-g}\left[\rho_0^2 + \frac{\pi gT^2}{a}\exp\left(-v_\tau^2T^2/4\right)\right], \end{aligned} \quad (8)$$

where η_0 is the characteristic impedance of free space, P_t is the radiated power of the transmitting antenna, $r_i\,(r_s)$ is the distance from the transmitting (receiving) antenna to A, $G_t(\theta_t, \phi_t)$ is the power gain of the transmitting antenna in the propagation direction (θ_t, ϕ_t) toward A, and $G_r(\theta_r, \phi_r)$ is the power gain of the receiving antenna in the propagation direction (θ_r, ϕ_r) toward A. The total scattered power is obtained by adding the scattered power from all the subareas within the illuminated area.

III. Ray Tracing Approach

The atmospheric refractivity affects the wave propagation. When air stratification is formed under stagnant weather, multiple propagation paths may exist in the atmosphere. Interference among these waves and the scattered waves from the terrain may cause signal fading. In this section, we briefly review the ray tracing approach by Shkarofsky and Nickerson [11].

A ray trace can be obtained by integrating the following two vector equations:

$$\begin{aligned}\frac{d\bar{r}}{d\xi} &= \bar{b} \\ \frac{d\bar{b}}{d\xi} &= \frac{1}{2}\nabla n^2, \end{aligned} \quad (9)$$

where ξ is the independent variable, $\bar{r}$ is the position vector of the ray trace, $\bar{b}$ is an auxiliary vector, and n is the refractive index in the atmosphere. We use Runge-Kutta's method of the fourth order to integrate (9), and use Newton-Raphson's method to search the ray trace between two fixed antennas [15]. The path length s, the phase Φ, and the polarization vector $\bar{e}$ can be obtained by integrating

$$\begin{aligned}\frac{ds}{d\xi} &= n \\ \frac{d\Phi}{d\xi} &= k_0n^2 \\ \frac{d\bar{e}}{d\xi} + \frac{1}{4}\bar{e}(\bar{b}\cdot\nabla\log n^2) + \frac{1}{2}\bar{b}(\bar{e}\cdot\nabla\log n^2) &= 0 \end{aligned} \quad (10)$$

along the ray trace. Here, k_0 is the wave number in free space.

To calculate the power density at the receiving antenna, we first deviate the launching angle of the ray trace infinitesimally in both the azimuthal and the elevation direction to form a ray bundle. Then, from the cross section variation of this ray bundle and the power conservation law, we obtain the power density at the receiving antenna. The refractive index $n(h)$ in the atmosphere can be expressed as

$$n(h) = 1 + 10^{-6}N(h), \tag{11}$$

where h is the height above sea level, and $N(h)$ is the refractivity at h. Because of temperature and humidity variations, anomalous refractivity may occur [9]. A typical anomalous refractivity can be described as [10]

$$N(h) = N_0 + \gamma h + \frac{\Delta N}{\pi}\tan^{-1}[12.63(h - h_0)/\Delta h], \tag{12}$$

where N_0 is the ground refractivity, γ is the medium refractivity gradient, ΔN is the anomaly intensity, Δh is the anomaly thickness, and h_0 is the anomaly height.

IV. Empirical Microwave Radio Models

Two empirical models are generally used to predict multipath fading distribution. In the United States, multipath fading data have been collected from many line-of-sight microwave links at 2, 4, 6, and 11 GHz. From these data, an empirical model has been derived to predict the distribution of multipath caused down-fade on microwave radio links as [5]

$$T_m = 0.4T_f c f d^3 10^{-F_c/10} \quad \text{s/yr/hop}, \tag{13}$$

where T_m is the accumulated seconds per year that the fade depth exceeds the given threshold, F_c, in dB, T_f is the average annual temperature in degrees Fahrenheit in the vicinity of the radio link, f is the radio frequency in GHz, d is the radio link length in miles, and c is the geoclimatic factor.

When the fade depth is greater than 10 dB, the multipath fading distribution drops by a factor of 10 for every 10 dB increase of fade depth. In [4], Lin analyzed the statistical behaviors of multipath fading and provided a theoretical basis for this observation.

The International Radio Consultative Committee (CCIR) proposes a similar model to calculate the fading probability at large fade depths as [16]

$$F(w) = Q(w/w_0)f^{\alpha}d^{\beta}, \tag{14}$$

where $F(w)$ is the probability that the received power is lower than w, f is the frequency in GHz, d is the path length in km, w is the received power in watts, w_0 is the received power in watts under normal atmospheric condition, and Q is the geoclimatic factor.

A recent study suggests that extrapolation of (13) and (14) to a lower frequency range is feasible for microwave link [17]. Therefore, we apply (13) and (14) to predict the microwave fading distribution at 450 MHz. Then we assume that a scaling factor can be derived to modify the empirical models in (13) and (14) for BEXR applications. The main differences between microwave links and BEXR links are the antenna heights and antenna beamwidths; hence the scaling factor should be a function of these two parameters. In the next two sections, we will first present results on BEXR by using the rough surface model and the ray tracing approach. Then, we will present simulation methods and results which lead to a scaling factor.

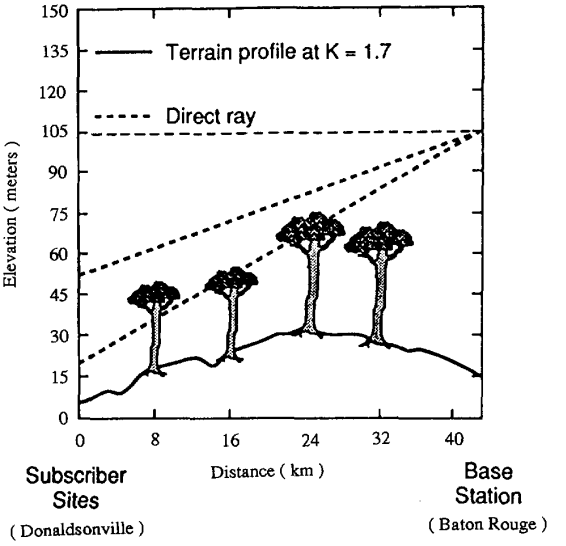

Fig. 2. Path profile of the basic exchange radio (BEXR) experiment between Baton Rouge and Donaldsonville, LA; path length is 43.2 km. $f = 454.375$ MHz, $h_t = 91.4$ m, $h_r = 48.2\,(15.2)$ m.

V. Modeling Results on BEXR

The Louisiana BEXR experiment was on a 43.2 km path from Baton Rouge to Donaldsonville [7], [13]. The terrain profile is obtained from a three-second digital terrain data base. The transmitting antenna at Baton Rouge is located at (30°26′59″N, 91°11′06″W), and the receiving antenna at Donaldsonville is located at (30°05′41″N, 90°59′54″W). The path profile between these two antennas is shown in Fig. 2.

The transmitting antenna at Baton Rouge is 91.4 m above ground level with a 4 dB gain and operates at 454.375 MHz. It has an omnidirectional radiation pattern in the horizontal plane and a half power beamwidth of 14° in the vertical plane. The two receiving antennas at Donaldsonville are 48.2 m (upper antenna) and 15.2 m (lower antenna) above the ground. They are Yagi antennas with 10 dB gain. The half power beamwidths are 60° in the vertical plane and 40° in the horizontal plane.

We also choose an imaginary microwave link for comparison. The transmitting (receiving) antenna is 84.8 (93.9) m above ground at the same site as the BEXR transmitting (receiving) antenna. We choose a typical number, 3°, as the beamwidth of both antennas in both the vertical and horizontal planes.

To calculate the terrain scattering, we first divide the whole terrain surface into three-second by three-second subareas. The received scattering power is the sum of the scattering powers from all subareas. For each subarea, the scattering power is calculated by using (8). We approximate the power gain,

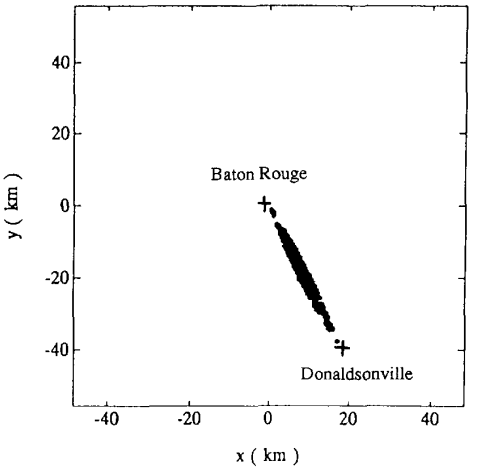

Fig. 3. The illuminated area of the microwave link from Baton Rouge to Donaldsonville based on the three-second terrain data base. $f = 454.375$ MHz, $h_t = 84.8$ m, $h_r = 93.9$ m; average tree height is 15 m.

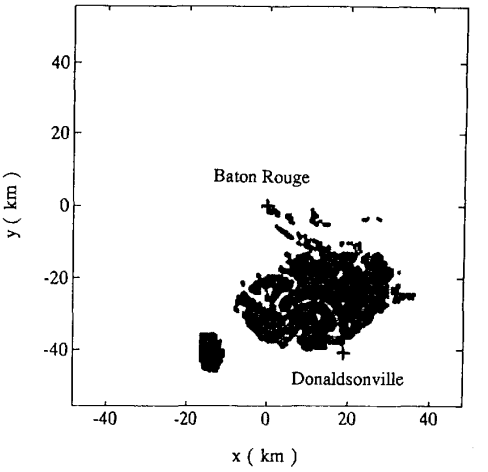

Fig. 4. The illuminated area of the upper BEXR link from Baton Rouge to Donaldsonville based on the three-second terrain data base. $f = 454.375$ MHz, $h_t = 91.4$ m, $h_r = 48.2$ m; average tree height is 15 m.

$G_t(\theta_t, \phi_t)$ by a joint Gaussian function as

$$G_t(\theta_t, \phi_t) = G_{t0} \exp\Big[-(\log_e 2) \cdot \Big((\theta_t - \theta_{t0})^2/\theta_{tm}^2 - (\phi_t - \phi_{t0})^2/\phi_{tm}^2\Big)\Big], \quad (15)$$

where G_{t0} is the antenna gain, (θ_{t0}, ϕ_{t0}) is the bore-sight direction of the transmitting antenna toward the subarea, $2\theta_{tm}$ and $2\phi_{tm}$ are the half power beamwidths in the vertical plane and the horizontal plane, respectively. The receiving antenna power gain, $G_r(\theta_r, \phi_r)$, is approximated in a similar way.

After calculating the scattering power from all the subareas, the maximum one is chosen as the power reference. The illuminated area consists of all the subareas, with each contributing at least 10^{-3} times the power reference. In Fig. 3, we show the illuminated area for the microwave link, which lies between the transmitting and receiving antennas.

In Fig. 4, we show the illuminated area for the upper BEXR link. Because of the wide beamwidth of the two antennas, the illuminated area is much wider than that of the microwave link. The blank strip indicates the river, which is obstructed from both antennas by the surrounding terrain.

In Fig. 5, we show the illuminated area for the lower BEXR link. The area is much smaller than that of the upper BEXR link because the receiving antenna is barely higher than the average tree height, which is estimated to be 15 m. Hence, most subareas are obstructed from the two antennas by the terrain.

In Fig. 6, we show the received power due to terrain scattering as a function of average tree height for all three links. As the tree height increases, the received power first increases due to reducing grazing angle, then decreases drastically because of tree obstruction.

In Fig. 7, we present the received power due to terrain scattering as a function of the effective earth radius factor, K. The average tree height is assumed to be 15 m. When

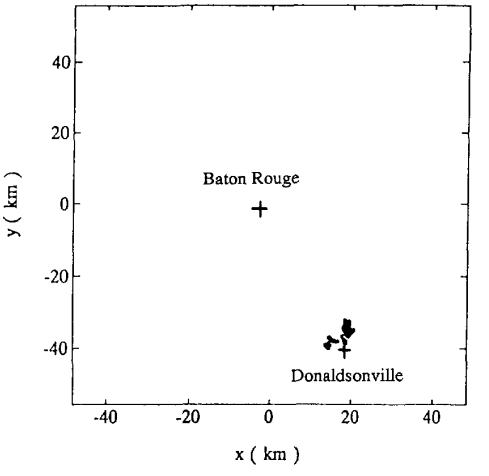

Fig. 5. The illuminated area of the lower BEXR link from Baton Rouge to Donaldsonville based on the three-second terrain data base. $f = 454.375$ MHz, $h_t = 91.4$ m, $h_r = 15.2$ m; average tree height is 15 m.

K becomes smaller, the grazing angles decreases and the scattering power increases. This phenomenon is more obvious for the lower BEXR link because of the lower receiving antenna height. When K is smaller than 1.6, the received power of the lower BEXR link drops drastically because of tree obstruction.

We also find that the scattering signal strength is insensitive to the terrain roughness and tree height. Because the grazing angles for the three links we consider are very low, only the tips of terrain irregularities are illuminated.

To study the air refraction, (12) is used to represent the anomalous refractivity in the atmosphere. To demonstrate our approach, we display in Fig. 8 a refractivity profile example as a function of height above sea level. We also display the

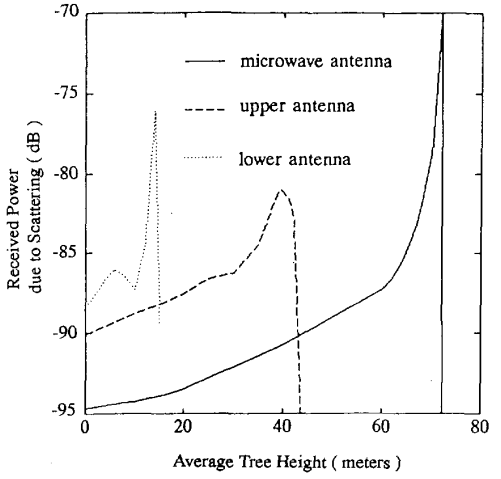

Fig. 6. The received power due to terrain scattering at different average tree heights obtained by the rough surface model. The transmitter power is used as power level reference.

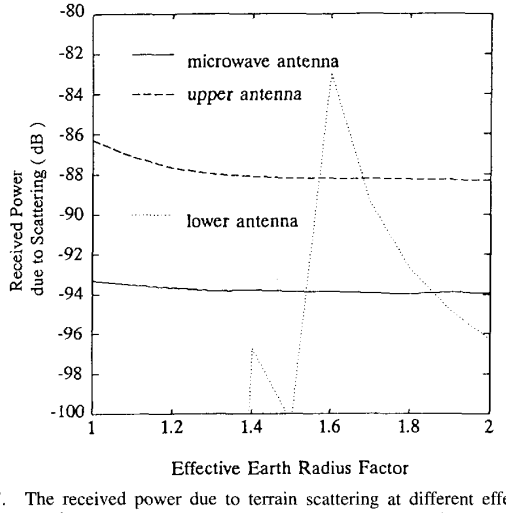

Fig. 7. The received power due to terrain scattering at different effective earth radius factors obtained by the rough surface model. The transmitter power is used as power level reference.

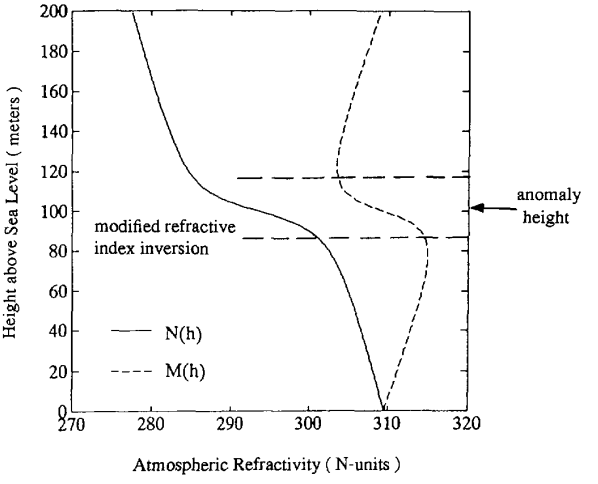

Fig. 8. Refractivity as a function of h described by (12) and (16). $N_0 = 300$ N-units, $\gamma = -65$ N-units/km, $\Delta N = -20N$-units, $\Delta h = 100$ m, $h_0 = 100$ m.

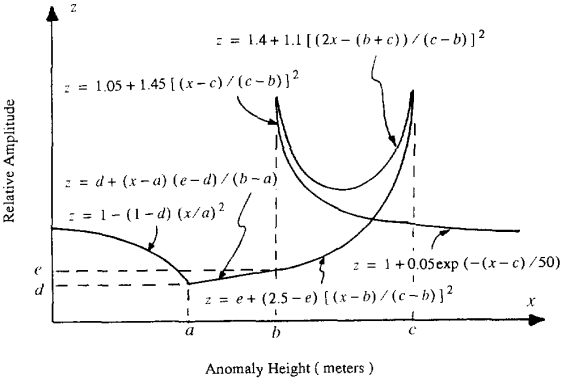

Fig. 9. Characterizing signal amplitudes of multipath propagation relative to a signal propagating in free space. Results are obtained by using the ray tracing approach for various γ, ΔN, Δh, and h_0.

modified refractive index, $M(h)$, which is related to $N(h)$ by

$$M(h) = N(h) + 10^6(h/a_e), \tag{16}$$

where a_e is the earth radius.

In Fig. 9, we show typical signal amplitudes of the multiple received rays for any of the three links relative to the magnitude of a ray traveling in free space. Three rays may occur within a range of anomaly height which is close to the region where the modified refractive index inversion occurs as shown in Fig. 8. The corresponding relative delay time is shown in Fig. 10. The parameters in these two figures will be discussed in the next section.

The received power due to terrain scattering is comparable to that of the air-refracted signal, especially for the BEXR links. Hence, we need to consider both signals in calculating the total received signal.

VI. Calculation of Scaling Factor

In this section, we will study the difference of fading distributions among the three links by simulation. Applying the terrain scattering model and the ray tracing approach directly in Monte-Carlo simulation is very time consuming. Hence, we try to characterize the scattering signal and the refractive signal by a set of parameters and then use these parameters to simulate the received signal.

We apply the method of Section III to calculate the signal amplitudes and delay times for various γ, ΔN, Δh, and h_0 and observe that they can be characterized as shown in Figs. 9 and 10. In these figures we observe the following relations

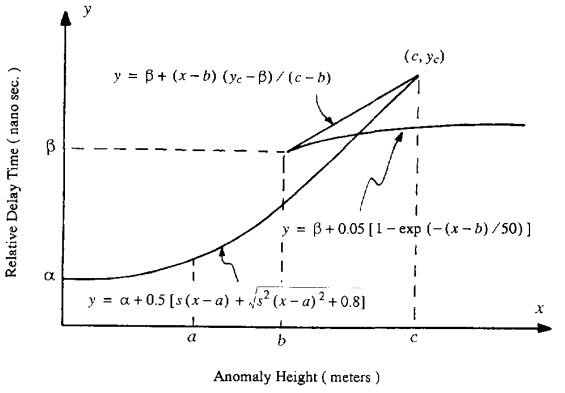

Fig. 10. Characterizing delay times of multipath propagation relative to a signal propagating in free space. Results are obtained by using the ray tracing approach for various γ, ΔN, Δh, and h_0.

among parameters:

$$a_m > a_u > a_l$$
$$b_m > b_u > b_l$$
$$b_m - b_u > b_u - b_l$$
$$c_m > c_u > c_l$$
$$c_m - b_m > c_u - b_u > c_l - b_l$$
$$(c_u - b_u)/(c_m - b_m) > (c_l - b_l)/(c_u - b_u)$$
$$d_m < d_u < d_l$$
$$\alpha_m < \alpha_u < \alpha_l$$
$$\beta_m < \beta_u < \beta_l$$
$$\alpha_m - \alpha_u \approx -0.22 \approx \alpha_u - \alpha_l$$
$$\beta_m - \beta_u \approx -0.22 \approx \beta_u - \beta_l$$
$$s_m \approx s_u \approx s_l,$$

where the subscripts m, u, and l stand for microwave link, upper BEXR link, and lower BEXR link, respectively. The correlations among the three links are partially accounted for by these relations.

In our simulation, the following parameters are chosen:

$$a_m = 80 \quad a_u = 50 \quad a_l = 20$$
$$b_m = A \quad b_m - b_u = 7 \quad b_u - b_l = 5$$
$$c_m - b_m = D \quad c_u - b_u = E(c_m - b_m)$$
$$c_l - b_l = (E - 0.15)(c_u - b_u) \quad d_m = 0.2$$
$$d_u = 0.3 \quad d_l = 0.4 \quad e_m = 0.3$$
$$e_u = 0.2 \quad e_l = 0.3 \quad \alpha_m = 0$$
$$\alpha_u = 0.22 \quad \alpha_l = 0.44 \quad \beta_m = G$$
$$\beta_u - \beta_m = 0.22 \quad \beta_l - \beta_u = 0.22$$
$$s_m = s_u = s_l = S$$

Now, the variables are reduced to A, D, E, G, S, and the anomaly height h_0. Their ranges are chosen to be $110 \le A \le 130$, $30 \le D \le 60$, $0.55 \le E \le 0.85$, $0.6 \le G \le 1.8$, $0.01 \le S \le 0.02$, and $0 \le h_0 \le 100$. We do not consider the fact that the occurrence of refractivity anomaly is less frequent at higher altitude [9].

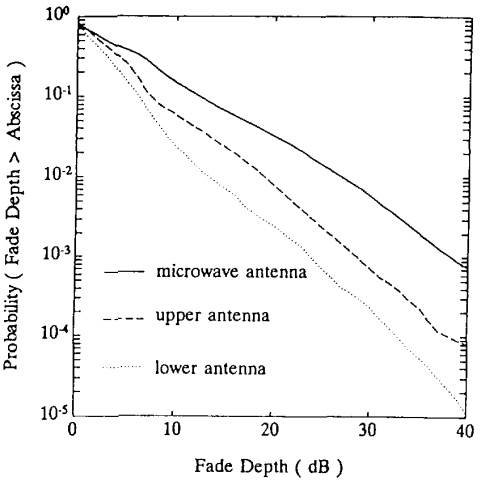

Fig. 11. Simulated fade depth distributions for the microwave link and the BEXR links.

Next, we combine the terrain scattering signal and the refracted signal. Since the scattering signal and the refractive signal propagate through different paths, and can be affected by phase delay mechanisms not described in our model [9], [18], [19], we assume that the phases of the terrain scattering signal and the refractive signal are uncorrelated.

Based on the results in Fig. 7, we choose the scattering signal between –93 dB and –94 dB for the microwave link, between –86 dB and –88 dB for the upper BEXR link, and between –83 dB and –88 dB for the lower BEXR link.

Although the variation of effective earth radius will focus or defocus the refractive rays while changing the terrain scattering signal, the correlation is not implemented in our simulation.

We assume that the parameters A, D, E, G, S, and h_0 are independent and uniformly distributed. Each parameter is varied from its minimum to maximum with a fixed increment. The increment size is reduced iteratively until the simulated fade depth distribution curves converge to those obtained with larger increments.

The simulated fade depth distribution curves are shown in Fig. 11. The distribution curve of the upper BEXR link is roughly parallel to that of the lower BEXR link. On the average, the curve of the microwave link is 5.9 dB (9.6 dB) above that of the upper (lower) BEXR link for fade depths greater than 10 dB. A possible reason that the microwave link has a higher probability of fading than the BEXR links is that the latter have a wider range of terrain scattering signal levels than the former; hence the combination of terrain scattering signal with refracted signals creates fewer occurrences of fades on the BEXR links. The same argument can be used when comparing the upper BEXR link with the lower one.

The fade depth distributions in Fig. 11 are obtained under anomalous refractivity conditions. We cannot get the absolute fade depth distribution unless we know the atmospheric refractivity distribution in the area. However, we can use the fade depth differences in Fig. 11 as scaling factors to modify

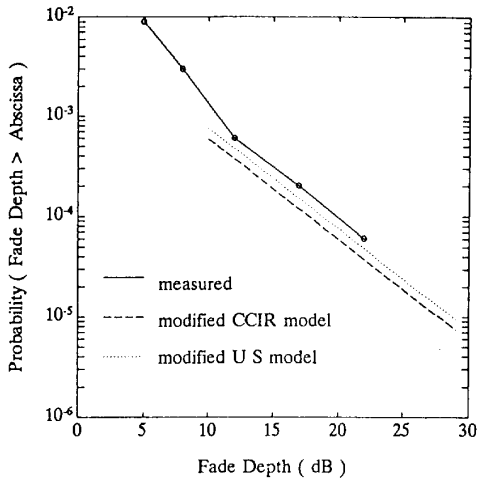

Fig. 12. Comparison of the measured fade depth distribution on the upper BEXR link with the modified empirical models.

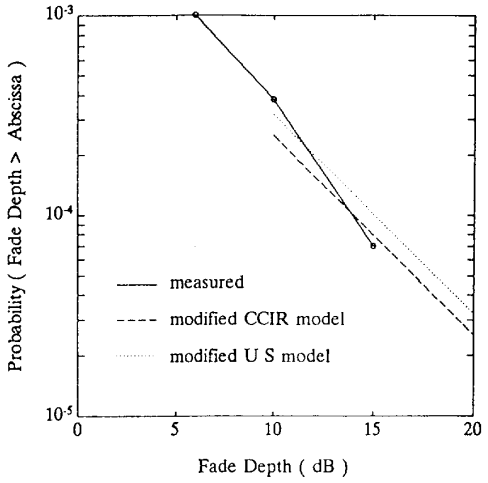

Fig. 13. Comparison of the measured fade depth distribution on the lower BEXR link with the modified empirical models.

the microwave empirical formula for BEXR links. These are called modified empirical models in the following figures.

The solid curves in Figs. 12 and 13 represent measured data which were collected from June to early October 1989 for the upper BEXR link and from July to September 1989 for the lower link. The received signal was sampled and recorded once every 2 s [7], [13]. In Fig. 12 (Fig. 13), we also show the modified empirical curves to compare with the measured distribution curve. The modified empirical curves match well with the measured results. We choose the average temperature during the measurement period to be $T_f = 65°\mathrm{F}$ and geoclimatic factor $c = 4$, $Q = 100$, $\alpha = 1$, and $\beta = 3$ in (13) and (14).

The scaling factor we developed improves the prediction by (13) or (14). However, the standard errors existing in (13) and (14) are not reduced by our scaling factor. This scaling factor is verified with one set of measurement data in the Baton Rouge area which is a plain full of trees and swamps. This simulation approach should be applicable to other areas and to different path profiles. However, the scaling factor will be different from case to case. More measurement data and studies are needed to obtain an empirical formula for the scaling factor.

VII. Conclusion

Due to significant differences in the antenna beamwidths and path clearance, the statistical behaviors of fading signals on the BEXR links differ from those on the microwave links. We present a method to obtain a scaling factor which accounts for the differences between the microwave fading distribution and the BEXR fading distribution. We first study the characteristics of terrain scattering by rough surface and of air refraction by anomalous refractivity. Then, simulations of received signals for a microwave link and two BEXR links are performed by combining the scattered and refracted signals. Finally, the scaling factors of fade depth distribution curves from the simulation results are used to modify the empirical microwave models to extend their applicability to BEXR links. The predictions by this modified empirical model agree well with the measured data and indicate that the fade depth distribution is a strong function of antenna height and antenna beamwidth.

Acknowledgment

The authors would like to thank W. J. Kish and his Bell-South colleagues for measuring BEXR fading distribution and J. Belcea at Bellcore for preparing the three-second digital terrain data in the Baton Rouge area. Thanks are also due to A. Ranade at Bellcore and to the anonymous reviewers in revising this paper.

References

[1] S. H. Lin and R. S. Wolff, "Basic exchange radio—From concept to reality," in *Proc. IEEE Int. Conf. Commun.* (Atlanta, GA), Apr. 1990, pp. 206.2.1–7.
[2] "Generic criteria for Basic Exchange Radio systems," Bellcore Technical Reference, TR-NWT-000 911, issue 1, Sept. 1990, Bellcore Customer Service, 60 New England Ave., Piscataway, NJ.
[3] "Radio systems operating in bands 8 and 9 for provision of subscriber telephone connections in rural areas," Int. Telecomm. Union CCIR Report 380–2, Dusseldorf, Geneva, 1990.
[4] S. H. Lin, "Statistical behavior of fading signal," *Bell Syst. Tech. J.*, vol. 50, no. 10, pp. 3211–3270, Dec. 1971.
[5] W. T. Barnett, "Multipath propagation at 4, 6, and 11 GHz," *Bell Syst. Tech. J.*, vol. 51, no. 2, pp. 321–361, Feb. 1972.
[6] A. Vigants, "Microwave radio obstruction fading," *Bell Syst. Tech. J.*, vol. 60, no. 6, pp. 785–801, July 1981.
[7] W. J. Kish, private communication.
[8] G. N. Patterson, "Fading characteristics of a geographically fixed, normally line of sight, 450 MHz radio channel in the southeastern United States," in *Proc. IEEE Int. Conf. Commun.* (Atlanta, GA), Apr. 1990.
[9] F. Ikegami, M. Haga, T. Fukuda, and H. Yoshida, "Experimental studies on atmospheric ducts and microwave fading," *Rev. Elec. Comm. Lab.*, vol. 14, no. 7, pp. 505–533, July 1966.
[10] A. R. Webster, "Angles-of-arrival and delay times on terrestrial line-of-sight microwave links," *IEEE Trans. Antennas Propagat.*, vol. 31, pp. 12–17, Jan. 1983.
[11] I. P. Shkarofsky and S. B. Nickerson, "Computer modeling of multipath propagation: Review of ray-tracing techniques," *Radio Sci.*, vol. 17, no. 5, pp. 1133–1158, Sept. 1982.

[12] E. Costa, "The effects of ground-reflected rays and atmospheric inhomogeneities on multipath fading," *IEEE Trans. Antennas Propagat.*, vol. 39, pp. 740–745, June 1991.
[13] J. F. Kiang and S. H. Lin, "Empirical modifications to microwave radio signal fading models for basic exchange radio," in *Proc. IEEE Int. Conf. Commun.* (Chicago, IL), June 1992, pp. 350.3.1–6.
[14] P. Beckmann and A. Spizzichino, *The Scattering of Electromagnetic Waves from Rough Surfaces*. Norwood, MA : Artech House, 1987, ch. 5.
[15] W. H. Press, B. P. Flannery, S. A. Teukolsky, and W. T. Vetterling, *Numerical Recipes: The Art of Scientific Computing*. Cambridge, England: Cambridge University Press, 1989, chs. 15 and 16.
[16] "Propagation data and prediction methods required for line-of-sight radio-relay systems," Int. Telecomm. Union CCIR Report 338–6, Dubrovnik, Geneva, 1990.
[17] R. L. Olsen and B. Segal, "New techniques for predicting the multipath fading distribution on VHF/UHF/SHF line-of-sight links in Canada," *Can. J. Elect. & Comp. Eng.*, vol. 17, no. 1, pp. 11–23, 1992.
[18] T. Tjelta, R. L. Olsen, and L. Martin, "Systematic development of new multivariable techniques for predicting the distribution of multipath fading on terrestrial microwave links," *IEEE Trans. Antennas Propagat.*, vol. 38, pp. 1650–1665, Oct. 1990.
[19] R. L. Olsen, L. Martin, and T. Tjelta, "A review of the role of surface reflection in multipath propagation over terrestrial microwave links," in *NATO/AGARD Conf. Proc.*, no. 407, 1987, pp. 2.1–23..

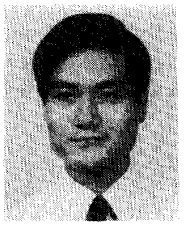

Jean-Fu Kiang (S'87–M'89) was born in Taipei, Taiwan, Republic of China on February 2, 1957. He obtained the B.S.E.E. and M.S.E.E. degrees from National Taiwan University in 1979 and 1981, respectively. He came to the Massachusetts Institute of Technology, Cambridge, in September 1983 as a research and teaching assistant and obtained the M.S.E.E. and Ph.D. degrees in electrical engineering in 1985 and March 1989, respectively.

He was with the Schlumberger-Doll Research Laboratory, Ridgefield, CT, for the summers of 1985 and 1986, the IBM T.J. Watson Research Center, Yorktown Heights, NY, from March 1989 to May 1990, and Bell Communications Research, Red Bank, NJ, from June 1990 to June 1992. He has been with the Siemens ElectroMedical Group, Danvers, MA, since July 1992.

Sing H. Lin (S'66–M'69–SM'87) received the Ph.D. degree from the University of California at Berkeley in 1969 and the B.S.E.E. degree from the National Taiwan University, Taipei, Taiwan, in 1963.

He is Director for PCS Planning and Wireless Access Technologies at Bellcore and leads a research team in developing generic requirements for wireless access communications systems. He has 23 years of experience in radio/wireless system engineering work and has published 51 technical papers in this field. His previous work involved basic exchange radio for rural telecommunications services, intercity microwave radio transmission systems, and cable transmission systems.

Dr. Lin is a member of the International Radio Consultative Committee (CCIR) and the International Scientific Radio Union (URSI). He is the holder of a patent and of a Bellcore Award of Excellence.